© 2015. Published by The Company of Biologists Ltd | Journal of Cell Science (2015) 128, 4407-4419 doi:10.1242/jcs.174359

RESEARCH ARTICLE

Sorting nexin 5 selectively regulates dorsal-ruffle-mediated macropinocytosis in primary macrophages

Jet Phey Lim, Prajakta Gosavi, Justine D. Mintern, Ellen M. Ross and Paul A. Gleeson*

ABSTRACT

The regulation of macropinocytosis, a specialised endocytosis pathway, is important for immune cell function. However, it is not known whether the biogenesis of macropinosomes involves one or more distinct pathways. We previously identified sorting nexin 5 (SNX5) as a regulator of macropinocytosis in macrophages. Here, we show that bone-marrow-derived macrophages from SNX5-knockout mice had a 60–70% reduction in macropinocytic uptake of dextran or ovalbumin, whereas phagocytosis and retrograde transport from the plasma membrane to the Golgi was unaffected. In contrast, deficiency of SNX5 had no effect on macropinocytosis or antigen presentation by dendritic cells. Activation of macrophages with CSF-1 resulted in a localisation of SNX5 to actin-rich ruffles in a manner dependent on receptor tyrosine kinases. SNX5-deficient macrophages showed a dramatic reduction in ruffling on the dorsal surface following CSF-1 receptor activation, whereas peripheral ruffling and cell migration were unaffected. We demonstrate that SNX5 is acting upstream of actin polymerisation following CSF-1 receptor activation. Overall, our findings reveal the important contribution of dorsal ruffing to receptor-activated macropinocytosis in primary macrophages and show that SNX5 selectively regulates macropinosomes derived from the dorsal ruffles.

KEY WORDS: Macropinocytosis, Sorting nexin, SNX5, Dorsal ruffle, Endocytosis, Antigen processing

INTRODUCTION

Macropinocytosis is a regulated pathway for the non-specific fluid-phase cellular uptake of extracellular fluid, solute molecules and antigens. Macropinocytosis is important in a wide range of cellular events including development, cell motility, tumour progression and metastasis (Lim and Gleeson, 2011; Swanson and Watts, 1995), provides an entry into the cell for a number of pathogens and mediates antigen sampling by antigen-presenting cells of the innate immune system (Mercer and Helenius, 2012; Norbury, 2006).

Macropinocytosis is an actin-dependent process initiated by surface membrane ruffles that give rise to large irregularly shaped endocytic vesicles with a diameter from >0.2 µm to 10 µm called macropinosomes (Hewlett et al., 1994; Swanson and Watts, 1995). A variety of membrane ruffles have been reported to give rise to macropinosomes by fusing with the plasma membrane. Macropinocytosis is a regulated endocytic process mediated by the activation of a variety of cell surface receptors including macrophage colony stimulating factor (CSF-1), epidermal growth factor (EGF) and platelet-derived growth factor (Dharmawardhane et al., 2000; Haigler et al., 1979; Racoosin and Swanson, 1989; Swanson, 1989). Phosphoinositides derived from receptor-mediated signalling events mediate the induction of macropinosomes (Amyere et al., 2000; Anzinger et al., 2012; Araki et al., 1996; Clague et al., 1995; Kerr et al., 2010; Yoshida et al., 2009). An important class of phosphoinositide effectors which regulate a variety of endocytic trafficking events, including macropinocytosis, are the sorting nexins (SNXs) (Cullen, 2008). A number of SNXs have been implicated in the biogenesis of macropinosomes, including SNX1, SNX5, SNX9, SNX18 and SNX33 (Lim et al., 2008; Wang et al., 2010). Our earlier studies have shown that SNX5 in particular is required for the early events in the formation of macropinosomes at the cell surface not only in cultured cells (Lim et al., 2008) but also primary macrophages (Lim et al., 2012). Following EGF stimulation of HEK293 cells, SNX5 is recruited to the plasma membrane and this recruitment is dependent on phosphatidylinositol (3,4)-bisphosphate (PIP_2) (Lim et al., 2008). Overexpression of SNX5 results in an increase in macropinocytosis in HEK293 cells (Lim et al., 2008), whereas silencing of SNX5 in bone-marrow-derived macrophages using microRNA results in a substantial decrease in the biogenesis of macropinosomes (Lim et al., 2012). Although SNX5 can form heterodimers with SNX1, we have previously shown that SNX5 can function independently of SNX1 (Lim et al., 2012). Hence, SNX5 appears to play a key role in the biogenesis of macropinosomes.

Macropinosomes can arise from distinct types of membrane ruffles, namely peripheral ruffles, which protrude from the leading edge that fold backwards, and dorsal ruffles, which are located on the dorsal surface of the cell. Dorsal ruffles have a distinctive circular or curved upright architecture, are very dynamic and appear transiently following receptor activation. In some cells, dorsal ruffles are specialised for initiating receptor signalling (Abella et al., 2010; Luo et al., 2014), for example dorsal ruffles are abundant in macrophages following activation (Patel and Harrison, 2008; Yoshida et al., 2009). Although macropinocytosis has been linked to both peripheral ruffles and dorsal ruffles, some reports have suggested that peripheral ruffles might be more relevant than dorsal ruffles for initiating macropinocytosis (Buccione et al., 2004; Hoon et al., 2012; Suetsugu et al., 2003). There remains uncertainty on the functional role of dorsal ruffles in macropinocytosis and the relative contribution of peripheral and dorsal ruffles to the macropinocytic pathway.

Macropinocytosis represents a major pathway by which innate immune cells capture antigens (Norbury et al., 1997, 1995; Sallusto et al., 1995). Professional antigen-presenting cells include dendritic cells and macrophages, and both these immune cells have high levels of macropinocytosis. Following antigen uptake, internalised antigens are processed into antigenic peptides, loaded onto major histocompatibility complex (MHC) molecules and the complex delivered to the cell surface for presentation to T-cells. However, a more detailed understanding of the macropinocytosis pathways in

The Department of Biochemistry and Molecular Biology and Bio21 Molecular Science and Biotechnology Institute, The University of Melbourne, Melbourne, Victoria 3010, Australia.

*Author for correspondence (pgleeson@unimelb.edu.au)

Received 18 May 2015; Accepted 5 October 2015

Journal of Cell Science (2015) 128, 4407-4419 doi:10.1242/jcs.174359

innate immune cells is required to appreciate the mechanism of antigen delivery and the ability to manipulate these pathways in the whole organism for functional analysis. In addition, it is not known whether the same regulators are relevant to macropinocytosis in both dendritic cells and macrophages. Given the importance of SNX5 in regulating the biogenesis of macropinosomes in macrophages, we have established a SNX5-knockout mouse line to investigate these questions. By analysis of macrophages and dendritic cells from *SNX5*$^{-/-}$ mice, here, we have demonstrated that SNX5 plays a specific role in the biogenesis of macropinosomes from dorsal ruffles and that dorsal ruffles provide a major contribution to macropinocytosis in activated macrophages.

RESULTS

SNX5$^{-/-}$ mouse line

The SNX5 'Knock-out First' mouse strain, was created from an embryonic stem cell (ESC) clone (a2EPD0033_3_D07) generated by the CHORI-Sanger-UC Davis (CSD) consortium for the NIH-funded knockout mouse project (KOMP). The mutant allele, which constitutes a knockout first allele (Skarnes et al., 2011), carries a modifiable gene-trap knockout first, lacZ-tagged insertion between exon 3 and exon 4 of *SNX5*. Homologous recombination results in the ablation of the *SNX5* allele by the insertion a SV40 polyadenylation (pA)-sequence-mediated transcriptional termination as part of the 5.5 kb non-genomic trapping cassette (Fig. 1A). Expression of exon 1 to exon 3 of *SNX5* would only result in a small~9.8 kDa protein representing the N-terminus of SNX5, which does not contain the lipid-binding phox (PX) domain. The SNX5 Knock-out First and control wild-type mice, on the same genetic background, will be referred to throughout the article as *SNX5*$^{-/-}$ and *SNX5*$^{+/+}$ mice, respectively. The *SNX5*$^{+/+}$ and *SNX5*$^{-/-}$ alleles were confirmed by PCR genotyping of mouse tail DNA (Fig. 1A,B).

The 50 kDa SNX5 protein was absent from bone-marrow-derived macrophages (BMMs) (Fig. 1C) and splenic dendritic cells from *SNX5*$^{-/-}$ mice (Fig. S1A), as determined by immunoblotting using an antibody that recognises the N-terminus of SNX5, and no smaller bands were detected. Whereas SNX5 protein was readily detected associated with endosomal structures in BMMs and dendritic cells from *SNX5*$^{+/+}$ mice, immunofluorescence analysis revealed that the punctate staining pattern attributed to endogenous SNX5 was absent in BMMs (Fig. 1D) and dendritic cells (Fig. S1B) from *SNX5*$^{-/-}$ mice.

There was no detectable abnormality in *SNX5*$^{-/-}$ mice compared to their wild-type counterparts. Both *SNX5*$^{-/-}$ and *SNX5*$^{+/+}$ mice

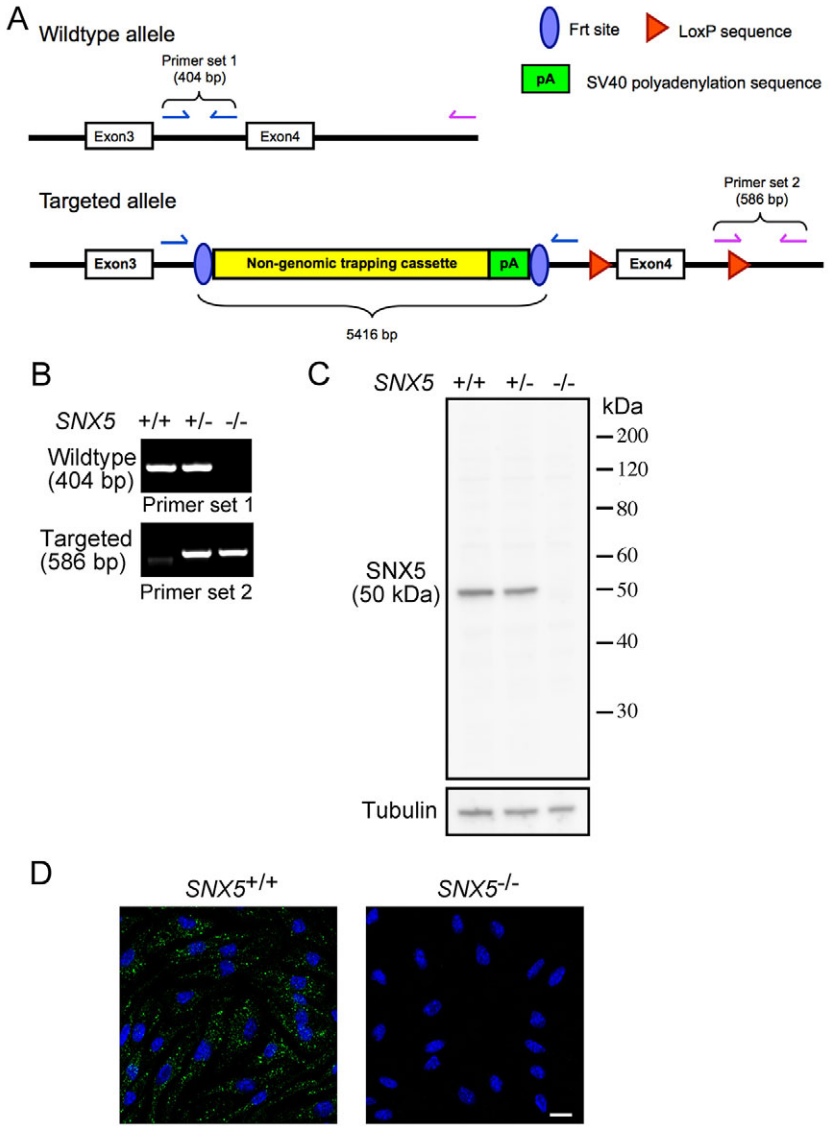

Fig. 1. Targeting the mouse SNX5 allele. (A) A non-genomic-trapping cassette carrying a SV40 polyadenylation sequence (which terminates transcription) was introduced into the *SNX5* allele between exon 3 and exon 4. (B) Genotype analysis of mice. *SNX5*$^{+/+}$ mice show a PCR product of 404 bp (top panel, far left) whereas *SNX5*$^{-/-}$ mice, with both copies of the *SNX5* allele targeted with the trapping cassette, show only a PCR product of 586 bp (bottom panel, far right). (C) SNX5 protein is not detected in *SNX5*$^{-/-}$ mice. BMMs from *SNX5*$^{+/+}$, *SNX5*$^{+/-}$ and *SNX5*$^{-/-}$ were lysed in reducing sample buffer and protein resolved on a 10% NuPAGE gel. Proteins were then transferred onto a PVDF membrane and probed with anti-SNX5 antibodies (top panel) and anti-α-tubulin was used a loading control (bottom panel). (D) BMMs were processed for immunofluorescence microscopy and stained using anti-SNX5 antibodies followed by Alexa-Fluor-488-conjugated anti-rabbit-IgG antibodies and DAPI. Punctate staining characteristic of endogenous SNX5 (left) was not detected in BMMs from *SNX5*$^{-/-}$ mice (right). Scale bar: 10 µm.

Journal of Cell Science (2015) 128, 4407-4419 doi:10.1242/jcs.174359

survived for >52 weeks (n=4 for $SNX5^{+/+}$ and $SNX5^{-/-}$) and were fertile with average litter sizes of 5.32 for $SNX5^{+/+}$ (n=25) and 5.62 for $SNX5^{-/-}$ (n=32). However, both male and female $SNX5^{-/-}$ mice were significantly smaller that $SNX5^{+/+}$ mice at 9 weeks±3 days ($SNX5^{+/+}$ male, 24.98±2.95 g; $SNX5^{-/-}$ male, 23.34±2.64 g; $SNX5^{+/+}$ female, 20.12±1.47; $SNX5^{-/-}$ female, 18.29±2.03; mean±s.d., n=38, 42, 29 and 32, respectively).

Macropinocytosis is substantially reduced in primary macrophages from *SNX5*$^{-/-}$ mice

Alterations in SNX5 expression either by RNA interference (RNAi)-mediated silencing of endogenous SNX5 (Lim et al., 2012) or elevated expression in HEK293 stable cell lines (Lim et al., 2008) alters macropinocytic activity. As macropinocytosis is considered an essential pathway for antigen sampling by antigen-presenting cells, we had anticipated that $SNX5^{-/-}$ mice might be immune-compromised; however, there was no evidence for an abnormal T cell compartment or viability of mice. Therefore, we investigated macropinocytosis activities in two major classes of antigen-presenting cells, macrophages and immature dendritic cells, from SNX5$^{-/-}$ mice.

BMMs were derived from $SNX5^{+/+}$ and $SNX5^{-/-}$ mice. Cells that had been rendered quiescent overnight were incubated with lysine-fixable, fluorescein isothiocynate (FITC)-conjugated 70 kDa dextran (FITC–dextran) in the presence of 50 ng/ml of CSF-1 for 15 min at 37°C to induce macropinocytosis. 70 kDa dextran is predominantly internalized by macropinocytosis (Kerr et al., 2006; Lim et al., 2012, 2008). Immunofluorescence analysis showed that endogenous SNX5 in CSF-1 activated BMMs from $SNX5^{+/+}$ mice is localised to endosomal structures (>500 nm in diameter) labelled with FITC–dextran (Fig. 2A) when BMMs were incubated at 37°C but not at 4°C, characteristics previously identified as macropinosomes (Lim et al., 2012). In contrast, $SNX5^{-/-}$ BMMs had significantly reduced FITC–dextran uptake when incubated with FITC–dextran at 37°C (Fig. 2B). The level of FITC–dextran intensity per μm^2 cell area was determined, using Metamorph software for >25 cells, and FITC–dextran uptake in $SNX5^{-/-}$ BMMs was reduced by 61% when compared to the wild-type counterpart (P<0.005) (Fig. 2C). Quantitative analysis by flow cytometry was also performed following fluid-phase FITC–dextran uptake for 15 min (Fig. 2D). A substantial reduction in the total uptake of FITC–dextran by $SNX5^{-/-}$ BMMs was observed compared with $SNX5^{+/+}$ BMMs, with a 50% reduction in median fluorescence intensity (four independent experiments) by $SNX5^{-/-}$ BMMs compared to $SNX5^{+/+}$ BMMs (Fig. 2D). The difference between microscopic and flow cytometry analysis is likely due to flow cytometry analysis measuring the total FITC–dextran level associated with cells whereas the microscopic analysis is restricted to intracellular macropinosome-associated FITC–dextran. The data collectively shows that SNX5 is required for efficient uptake of 70 kDa dextran by macropinocytic activity in BMMs.

Macropinocytosis is a major internalisation route for soluble antigen (Lim et al., 2012), and the subsequent processing of protein antigens in acidic intracellular compartments is an essential step in antigen presentation. To study antigen uptake and processing in the late endosomes and lysosomes, we used a self-quenched conjugate of ovalbumin, namely DQ-ovalbumin, which exhibits fluorescence only after proteolytic degradation (Daro et al., 2000; Santambrogio et al., 1999). BMMs from $SNX5^{+/+}$ and $SNX5^{-/-}$ mice that had been rendered quiescent overnight were pulsed with DQ-ovalbumin for 3 min in the presence of 50 ng/ml CSF-1 and then chased at 37°C for 30 min, the time required for ovalbumin to reach LAMP-1-positive compartments (Lim et al., 2012). Immunofluorescence analysis showed that BMMs from $SNX5^{-/-}$ mice had significantly reduced DQ-ovalbumin fluorescence intensity compared with cells incubated with DQ-ovalbumin at 4°C (Fig. 2E). Quantitative analysis of >25 BMMs showed 67% reduction (P<0.005) in DQ-ovalbumin fluorescent intensity in $SNX5^{-/-}$ BMMs compared with BMMs from $SNX5^{+/+}$ mice (Fig. 2F). The reduction in DQ-ovalbumin uptake and processing in $SNX5^{-/-}$ BMMs parallels the reduced macropinocytic activity. These data show that SNX5 regulates antigen uptake and processing by primary macrophages.

Macropinocytosis and antigen presentation is not affected in dendritic cells by the absence of SNX5

Given the importance of SNX5 in regulating macropinocytosis in macrophages, we anticipated that immature dendritic cells, which are specialised for antigen capture as they have a high macropinocytic activity (Lim and Gleeson, 2011; Norbury, 2006), might also be compromised in the absence of SNX5. The level of endogenous SNX5 protein in purified, splenic dendritic cells isolated from $SNX5^{+/+}$ mice is comparable to the level of SNX5 in $SNX5^{+/+}$ BMMs (Fig. 3A). To investigate whether SNX5 has a role in regulating macropinocytosis in dendritic cells, immature splenic dendritic cells were isolated from $SNX5^{+/+}$ and $SNX5^{-/-}$ mice as described in the Materials and Methods. Immature dendritic cells are highly endocytic and capture fluid-phase antigens by macropinocytosis and express relatively low levels of CD86 compared with activated mature dendritic cells (Villadangos and Schnorrer, 2007). Enriched populations of immature dendritic cells were incubated with FITC–dextran for 30 min at 37°C, or on ice, before excess FITC–dextran was removed. Dendritic cells were identified by staining for CD11c (encoded by *ITGAX*) and MHCII, and analysed by immunofluorescence after cytospin collection on glass slides. Dendritic cells from $SNX5^{+/+}$ and $SNX5^{-/-}$ mice internalised FITC–dextran (Fig. 3B) at 37°C but not on ice (4°C). To quantify the level of FITC–dextran uptake, flow cytometry analysis was performed on dendritic cells suspensions after fluid-phase FITC–dextran uptake. Cells were stained and immature dendritic cells identified using a combination of anti-CD11c, anti-CD86 and anti-MHCII antibodies. Immature dendritic cells (CD11c$^+$, MHCII$^+$, CD86^{low}) from $SNX5^{+/+}$ and $SNX5^{-/-}$ mice showed a similar intensity of FITC–dextran (Fig. 3B,C). These data indicate that macropinocytosis in immature dendritic cells is unaffected by the absence of SNX5. We also performed T cell proliferation assays to determine the efficacy of antigen presentation by dendritic cells from $SNX5^{-/-}$ mice using soluble ovalbumin as the fluid-phase antigen. Ovalbumin$_{323\text{-}339}$-specific (H-2^b) CD4$^+$ T cells (OTII) responded in a similar manner to ovalbumin-loaded splenic dendritic cells from $SNX5^{+/+}$ and $SNX5^{-/-}$ mice (data not shown), indicating that antigen uptake, processing and loading onto MHCII molecules is unaffected by the lack of SNX5 in dendritic cells. Collectively, and in contrast to primary macrophages, these data indicate that SNX5 does not regulate macropinocytosis in immature dendritic cells.

Lack of SNX5 does not affect phagocytosis or M6PR trafficking in macrophages

Having established that SNX5 plays an important role in macropinocytosis in BMMs, we sought to determine whether the impact of SNX5 is restricted to macropinocytosis or whether SNX5 is also relevant to other endocytosis pathways in macrophages. First, we assessed the phagocytic activity of SNX5-deficient

Journal of Cell Science (2015) 128, 4407-4419 doi:10.1242/jcs.174359

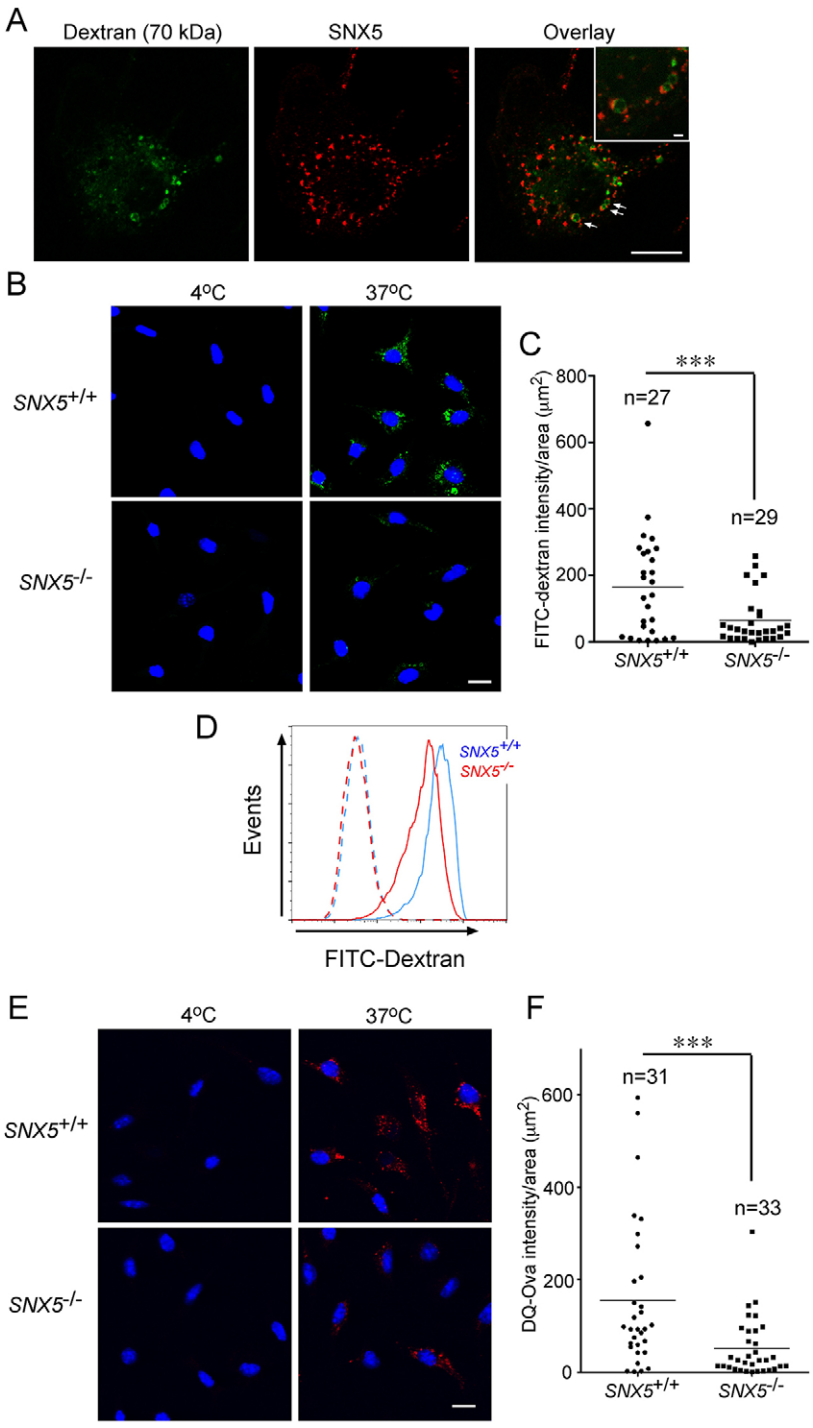

Fig. 2. Absence of SNX5 reduces macropinocytosis in BMMs. (A) SNX5 is localised on newly formed macropinosomes. Quiescent $SNX5^{+/+}$ BMMs were incubated with 500 µg/ml of FITC-conjugated 70 kDa dextran in the presence of 50 ng/ml CSF-1 for 15 min at 37°C. Monolayers were fixed, permeabilised and stained with rabbit anti-SNX5 antibodies (red). Macropinosomes are indicated by arrows. Macropinosomes indicated by arrows are magnified in the inset. Scale bars: 10 µm (main panel); 1 µm (inset). (B,C) Quiescent BMMs from $SNX5^{+/+}$ and $SNX5^{-/-}$ mice were incubated with 500 µg/ml FITC-conjugated 70 kDa dextran and 50 ng/ml CSF-1 for 15 min and fixed and processed. Scale bar: 10 µm. In C, the level of FITC–dextran uptake was analysed using Metamorph software. The mean is indicated. (D) Analysis of FITC–dextran uptake as in B by flow cytometry. 20,000 events were collected per sample. Dashed lines, cells incubated at 4°C on ice, solid lines, cells incubated at 37°C. (E,F) Quiescent BMMs from $SNX5^{+/+}$ and $SNX5^{-/-}$ mice were pulsed with 50 µg/ml DQ-ovalbumin in the presence of CSF-1 for 3 min, washed and chased for 30 min at 37°C in the presence of CSF-1 or incubated with DQ-ovalbumin in the presence of CSF-1 for 30 min on ice (4°C). Scale bar: 10 µm. In F, level of DQ-ovalbumin uptake was analysed using Metamorph software; the mean is indicated. ***P<0.001 (Student's t-test).

macrophages, as phagocytosis and macropinocytosis share some similarities such actin-dependence, formation of large vascular endocytic structures and common regulators, such as phosphoinositide 3-kinase (PI3K) and Rab5 (Feliciano et al., 2011; Lee and Knecht, 2002; May and Machesky, 2001; Roberts et al., 2000). To monitor phagocytic activity, $SNX5^{+/+}$ and $SNX5^{-/-}$ BMMs were incubated with Alexa-Fluor-488-labelled zymosan A bioparticles for 60 min at 37°C at two different concentrations. Zymosan particles were internalised efficiently into both $SNX5^{+/+}$ and $SNX5^{-/-}$ BMMs (Fig. 4A). The average number of zymosan particles per macrophage was similar for $SNX5^{+/+}$ BMMs [5.9±1.2 zymosan particles; mean±s.d., n=3 (50 cells each)] and $SNX5^{-/-}$ BMMs [6.7±0.8 zymosan particles, n=3 (50 cells for each)] at the higher concentration of 7×10^5 zymosan particles/ml, and 2.2±0.4 and 2.2±0.5 zymosan particles per cell for $SNX5^{+/+}$ and $SNX5^{-/-}$ BMMs, respectively, at 1.6×10^5 zymosan particles/ml (Fig. 4B). Staining of zymosan-loaded $SNX5^{-/-}$ BMMs with antibodies to SNX5 showed that SNX5 was absent from phagosome structures (data not shown). Therefore, these data show that SNX5 does not play a role in macrophage phagocytosis.

SNX5 has been suggested to have a role in retromer-mediated endosomal sorting and transport of cargo to the Golgi (Wassmer et al., 2007, 2009). To determine whether the lack of SNX5 in macrophages has an effect on retrograde transport, we assessed the

Journal of Cell Science (2015) 128, 4407-4419 doi:10.1242/jcs.174359

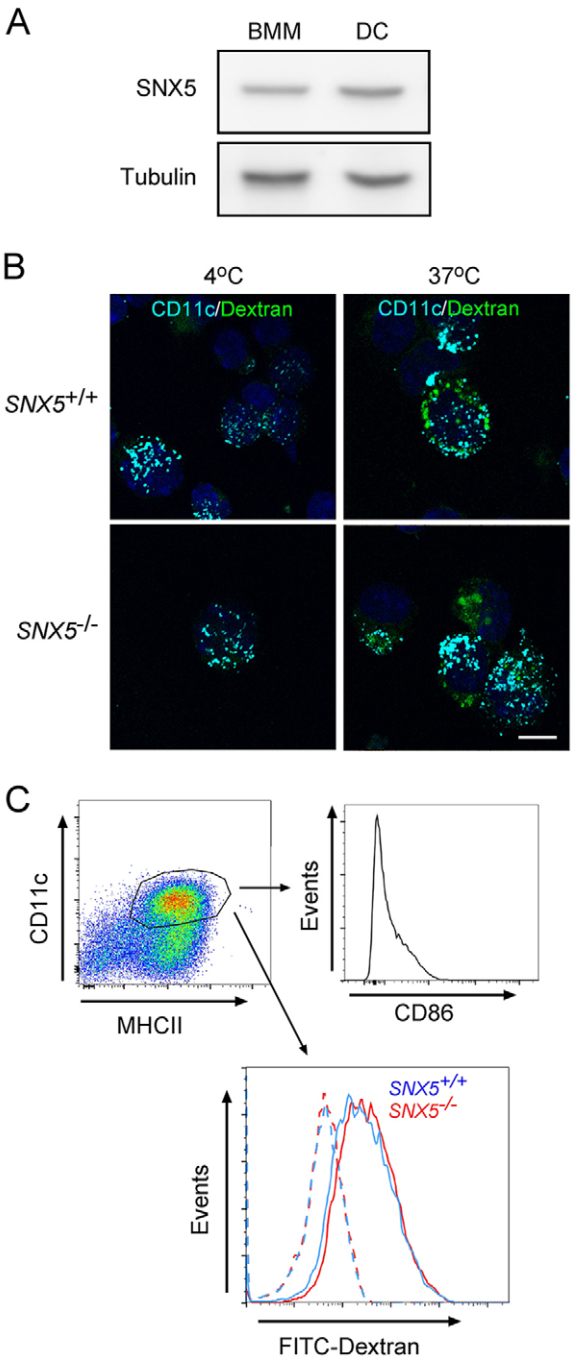

Fig. 3. Absence of SNX5 does not affect macropinocytosis in immature splenic dendritic cells. (A) Immunoblot of BMMs and purified splenic dendritic cells (DC) from *SNX5*$^{+/+}$ mice. BMMs and dendritic cells were lysed in a reducing sample buffer and samples were resolved in a 10% NuPAGE gel. Proteins were then transferred onto a PVDF membrane and probed with anti-SNX5 (top panel) and anti-α-tubulin (bottom panel) antibodies as a loading control. (B) Immunofluorescence images and (C) flow cytometry histogram of Nycodenz-enriched dendritic cells from *SNX5*$^{+/+}$ and *SNX5*$^{-/-}$ mice following incubation with 1 mg/ml of FITC-conjugated 70 kDa dextran at 37°C for 15 min and live cells stained with (B) biotinylated hamster anti-mouse CD11c antibody followed by streptavidin conjugated with Alexa Fluor 647 and DAPI prior to cytospin and microscopy or (C) stained with anti-CD11c antibody conjugated to eFluor® 450, anti-CD86 antibody conjugated to APC and anti-MHCII antibody conjugated to PerCP-Cy5.5. Shown are flow cytometric plots gated on CD11c^{+}, MHCII dendritic cells and analysed for CD86 expression and FITC–dextran update. Solid lines, cells incubated with dextran at 37°C; dashed lines, cells incubated with dextran at 4°C. Scale bar: 10 µm.

trafficking of the cation-independent mannose-6-phosphate receptor (M6PR, also known as IGF2R), which is recycled via endosomes and the Golgi. For this experiment, we used a CD8 chimera of M6PR (CD8–M6PR), previously used to analyse the internalisation of M6PR from the plasma membrane to early endosomes, followed by the intracellular transport, in a retromer-dependent manner, to the Golgi (Lieu et al., 2007; Seaman, 2004). The trafficking of the CD8–M6PR was analysed in recombinant adenovirus-transduced BMMs using an internalisation assay by tagging cell surface cargo with antibodies to the CD8 domain. Rapid internalisation of surface antibody-conjugated CD8–M6PR to endosomal structures in both *SNX5*$^{+/+}$ and *SNX5*$^{-/-}$ macrophages was detected within 5 min of incubation at 37°C. By 60 min incubation, the majority of the CD8–M6PR was detected in the Golgi region of both *SNX5*$^{+/+}$ and *SNX5*$^{-/-}$ macrophages (Fig. 4C,D). Hence the deficiency of SNX5 appears to have no effect on clathrin-mediated endocytosis and retrograde endosome to Golgi transport of M6PR, highlighting a specific role for SNX5 in macropinocytosis in BMMs.

SNX5 is located at the cell surface of macrophages following CSF-1 receptor activation

We have previously demonstrated that SNX5 is recruited to membrane ruffles of EGF-activated HEK293 cells expressing GFP–SNX5 (Lim et al., 2008). To determine whether SNX5 behaved in a similar manner in primary macrophages, we investigated the localisation of either endogenous or GFP-tagged SNX5 in CSF-1 activated *SNX5*$^{+/+}$ BMMs. In resting macrophages, where there are minimal actin-rich membrane ruffles, SNX5 is located predominantly in early endosomes (Fig. 1D; Lim et al., 2012). In contrast, CSF-1-activated macrophages showed the presence of actin-rich plasma membrane ruffles with strong colocalisation of SNX5 with actin (Fig. 5A) and with CSF-1 receptors on membrane ruffles (Fig. 5B). We assessed the influence of CSF-1 receptor signalling on macropinocytosis using GW2580, a specific CSF-1 receptor tyrosine kinase inhibitor. GW2580 treatment dramatically reduced FITC–dextran uptake of both *SNX5*$^{+/+}$ and *SNX5*$^{-/-}$ BMMs (Fig. 5C). For *SNX5*$^{+/+}$ BMMs, there was a 89% reduced uptake of FITC–dextran following GW2580 treatment. As expected, *SNX5*$^{-/-}$ BMMs had a reduced level of macropinocytosis compared with *SNX5*$^{+/+}$ BMMs in the presence of the carrier alone and this residual 30% macropinocytic activity was further reduced in the presence of GW2580 (Fig. 5C) to a similar level observed in *SNX5*$^{+/+}$ BMMs in the presence of GW2580. This finding shows that macropinocytosis in CSF-1-activated macrophages is regulated by the tyrosine kinase activity of the CSF-1 receptor and influenced by SNX5. The levels of CSF-1 receptor at the cell surface of *SNX5*$^{+/+}$ and *SNX5*$^{-/-}$ BMMs were similar (Fig. 5D), indicating that SNX5 is acting downstream of receptor activation to promote macropinocytosis.

Deficiency in SNX5 results in reduction of dorsal ruffling

Macropinosomes are derived from plasma membrane ruffles. Treatment of macrophages with CSF-1 has been shown to stimulate actin polymerisation (Sampaio et al., 2011), which is essential for macropinocytosis as well as chemotaxis (Jones, 2000). Given the possible link between macropinocytosis and chemotaxis, we investigated whether the reduced macropinocytic activity in *SNX5*$^{-/-}$ BMMs affected the chemotactic response of macrophages towards CSF-1 using a transwell migration assay. The results showed that *SNX5*$^{-/-}$ BMM migration (migration index of 1.55 and 1.55 in two separate experiments) was not significantly perturbed in their ability to migrate through the transwell compared with *SNX5*$^{+/+}$ BMMs

Journal of Cell Science (2015) 128, 4407-4419 doi:10.1242/jcs.174359

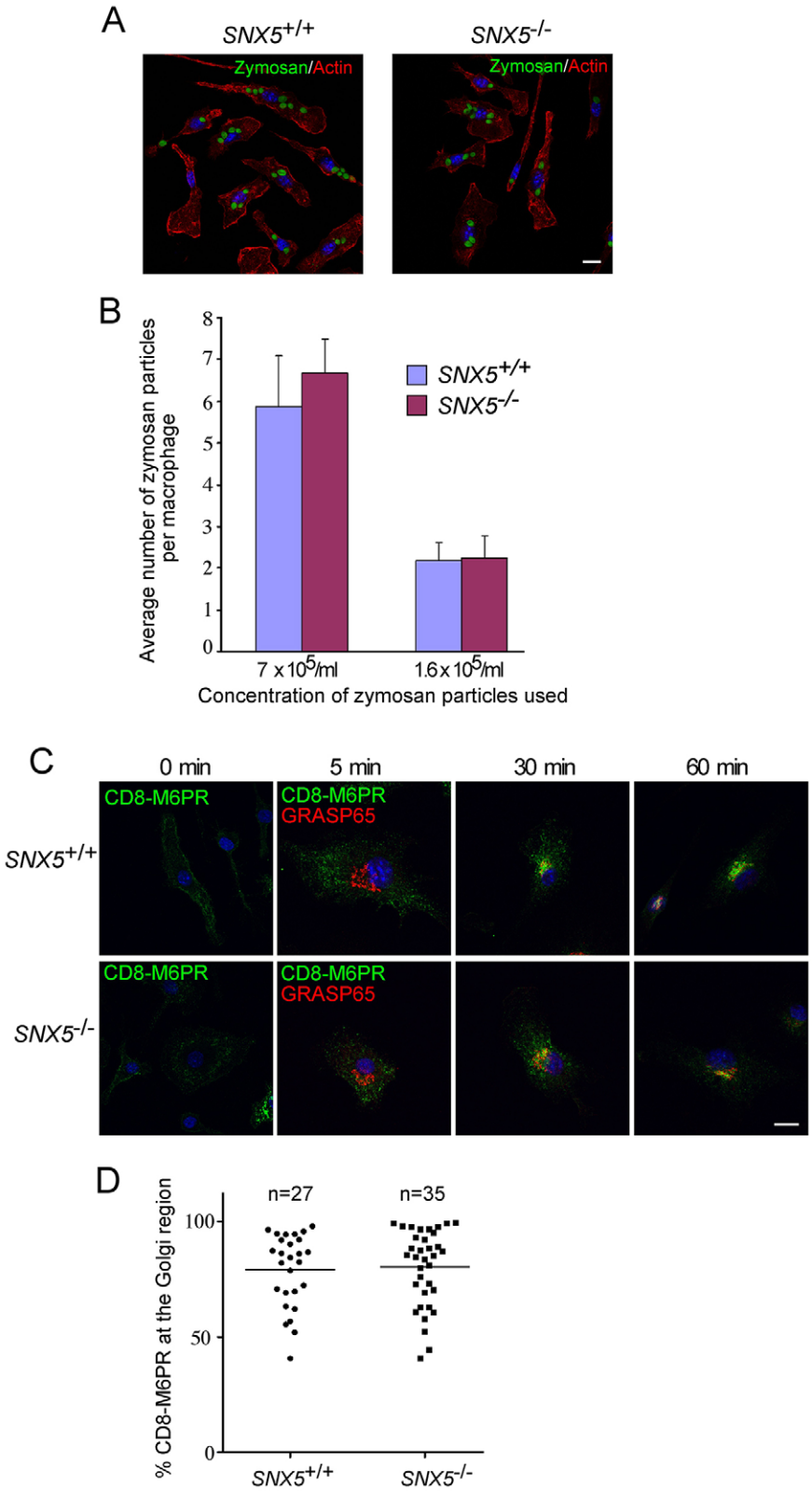

Fig. 4. Absence of SNX5 does not affect phagocytosis or retromer transport of CD8–M6PR. (A,B) BMMs from *SNX5*$^{+/+}$ and *SNX5*$^{-/-}$ mice were incubated with Alexa-Fluor-488-labelled zymosan A bioparticles at 37°C for 60 min. Non-phagocytosed zymosan particles were removed with ice-cold PBS washes. BMMs were (A) processed for immunofluorescence and stained with TRITC–phalloidin (red) followed by DAPI (blue). Scale bar: 10 µm. In B, the mean±s.d. of fluorescent particles per cell were scored for triplicate experiments of 50 cells each. Phagocytosis was expressed as the mean of particles per cell. (C,D) Expression of CD8–M6PR was introduced into BMMs by recombinant adenovirus. Prior to labelling with anti-CD8, BMMs was incubated with mouse BD Fc Block™. The internalisation and transport of the antibody–CD8–M6PR complex from the plasma membrane to the Golgi was tracked by incubation at 37°C for the indicated time. Monolayers were then fixed, permeabilised and stained with Alexa-Fluor-488-conjugated anti-mouse-IgG, anti-GRASP65 (where indicated) (red) and DAPI (blue). Scale bar: 10 µm. (D) Percentage of antibody-CD8-M6PR at the Golgi region after 60 min incubation at 37°C, determine by calculating the percentage of total pixels which overlapped with GRASP65 using Metamorph software. The mean is indicated.

(migration index of 1.23 and 1.36 in two separate experiments) suggesting that SNX5 is required for macropinocytosis but not for the chemotactic response of macrophages to CSF-1.

Macropinocytosis and chemotaxis require plasma membrane ruffling. There are three types of membrane ruffling: lamellipodia or sheet-like, dorsal ruffles and membrane blebbing (Mercer and Helenius, 2012). Of the three types, only lamellipodia ruffles, which normally occur at the leading edge of cells, and dorsal ruffles have been implicated in fluid-phase uptake and macropinosome formation. Thus, we investigated whether the regulation of macropinocytosis by SNX5 was associated with the initial formation of plasma membrane ruffles. To do this, we monitored

Journal of Cell Science (2015) 128, 4407-4419 doi:10.1242/jcs.174359

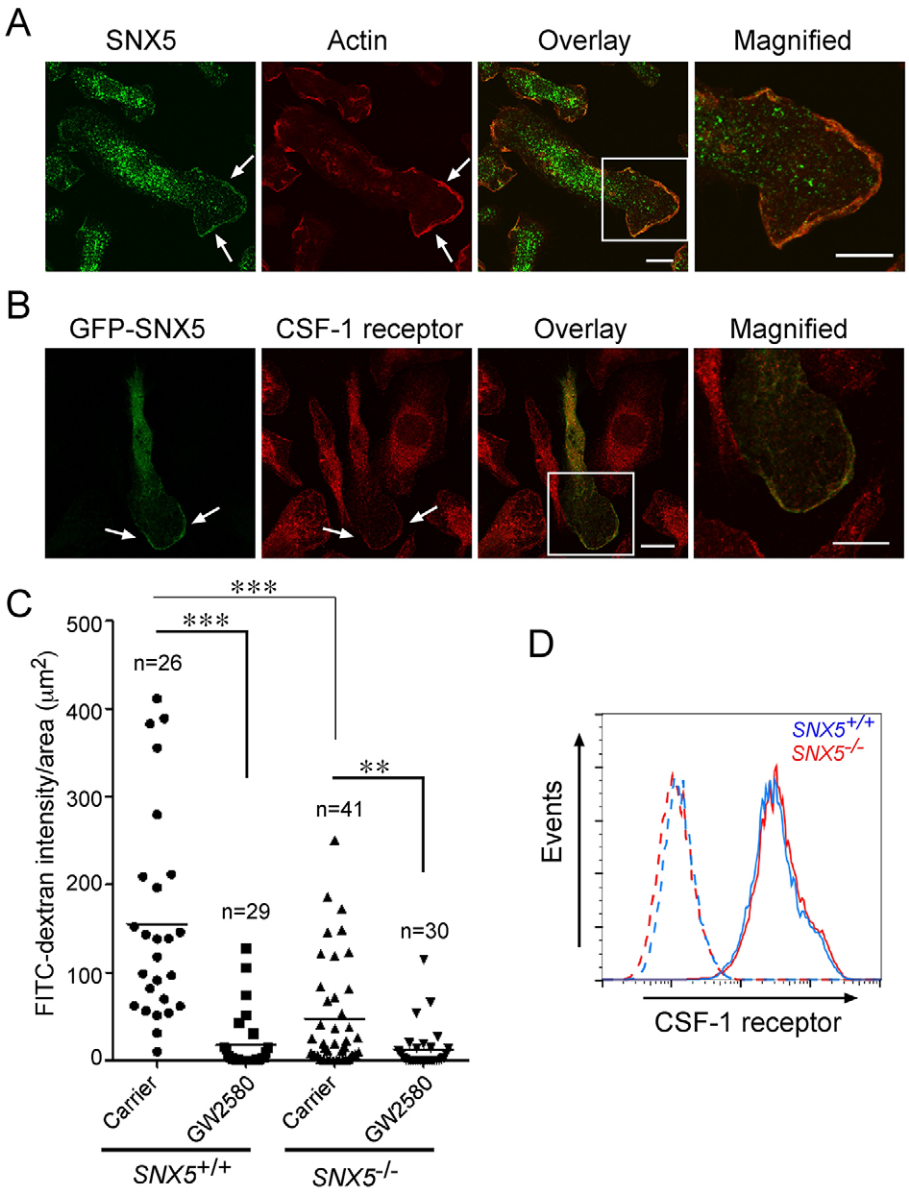

Fig. 5. SNX5 is localised to actin-rich plasma membrane ruffles in response to CSF-1 stimulation. (A) Endogenous SNX5 is localised on actin-rich regions of plasma membrane. Quiescent $SNX5^{+/+}$ BMMs were stimulated with CSF-1 for 3 min at 37°C, and monolayers then fixed, permeabilised and stained with either anti-SNX5 antibody followed by Alexa-Fluor-488-conjugated anti-rabbit-IgG antibody and TRITC–phalloidin (red). Arrows indicate regions of actin-rich plasma membrane ruffles. The boxed region is magnified on the far right. Scale bars: 10 µm. (B) SNX5 is localised with CSF-1 receptor at the plasma membrane. GFP-SNX5 was introduced into BMMs by recombinant adenovirus. Transduced BMMs were rendered quiescent overnight followed by 3 min stimulation with CSF-1 at 37°C, and monolayers then fixed, permeabilised and stained for CSF-1 receptor (red). Arrows indicate regions of plasma membrane where colocalisation is observed between GFP–SNX5 and CSF-1 receptor. Boxed region is magnified on the far right. Scale bars: 10 µm. (C) Effect of GW2580 on macropinocytosis in BMMs from $SNX5^{+/+}$ and $SNX5^{-/-}$ mice. Quiescent BMMs from $SNX5^{+/+}$ and $SNX5^{-/-}$ mice were pre-treated with 5 µM of GW2580 or DMSO carrier control for 1 h at 37°C. Cells were then incubated with 500 µg/ml of FITC-conjugated 70 kDa dextran and 50 ng/ml CSF-1 in the absence or presence of GW2580 (as indicated) for 15 min at 37°C prior to processing for immunofluorescence microscopy. Level of FITC-dextran uptake was analysed using Metamorph software. The mean is indicated. $^{**}P<0.01$, $^{***}P<0.001$ (Student's *t*-test). (D) Level of cell surface CSF-1 receptor in $SNX5^{+/+}$ and $SNX5^{-/-}$ BMMs. Quiescent BMMs were gently removed from petri dishes, stained for CSF-1 receptor followed by Alexa-Fluor-488-conjugated anti-rabbit-IgG antibody (solid lines) and 20,000 live cells were analysed by flow cytometry. Dashed lines, cells stained with conjugate alone.

the extent of ruffling in SNX5-deficient macrophages following CSF-1 activation. BMMs that had been rendered quiescent overnight were morphologically elongated with small protrusive areas at one or both ends of the cell (Fig. 6A). Stimulation with CSF-1 for 3 min at 37°C resulted in flattened $SNX5^{+/+}$ and $SNX5^{-/-}$ macrophages and the formation of planar lamellipodia with increased peripheral ruffling as indicated by an increase in F-actin intensity (Fig. 6A).

To investigate the formation of membrane ruffles on the dorsal surface of macrophages, two approaches were employed; an *x-z* series of confocal images and scanning electron microscopy (SEM). As assessed by confocal microscopy, CSF-1 activation of $SNX5^{+/+}$ BMMs resulted in considerable actin-stained projections from the dorsal surface of the cell (Fig. 6B; Movies 1 and 2). In contrast, very few actin projections were detected on the dorsal surface of CSF-1 treated $SNX5^{-/-}$ BMMs (Fig. 6B; Movies 3 and 4) and any actin projections detected from the dorsal surface were considerably smaller than those in $SNX5^{+/+}$ BMMs. Scanning electron microscopy clearly demonstrated the presence of dorsal ruffles on $SNX5^{+/+}$ BMMs following CSF-1 stimulation (Fig. 7A). In contrast, dorsal ruffles were dramatically reduced on CSF-1-stimulated $SNX5^{-/-}$ BMMs. Quantification of the extent of total membrane ruffling on SEM images was estimated by manually tracing the perimeter of the ruffles and measuring the area (Fig. 7B). There was a 68% and 71% reduction in total membrane ruffling in $SNX5^{-/-}$ BMMs, compared with $SNX5^{+/+}$ BMMs, after 3 min and 15 min CSF-1 stimulation, respectively (Fig. 7B). The reduction in membrane ruffling correlated with the level of reduction in macropinocytic activity in $SNX5^{-/-}$ BMMs (Fig. 2C). Therefore $SNX5^{-/-}$ BMMs have reduced dorsal membrane ruffling and macropinocytosis in response to CSF-1, whereas peripheral ruffling and cell migration is unaffected by the absence of SNX5.

To confirm that the deficiency of dorsal ruffles of $SNX5^{-/-}$ BMMs is a direct consequence of the lack of SNX5 protein, a rescue experiment was performed to re-introduce full-length SNX5 into $SNX5^{-/-}$ BMMs. BMMs from $SNX5^{-/-}$ mice were transduced with recombinant adenovirus which encodes GFP–SNX5. By performing quantitative immunofluorescence, we observed that transduced GFP-positive BMMs from $SNX5^{-/-}$ mice showed an equivalent or greater number of Texas-Red–dextran-labelled

Journal of Cell Science (2015) 128, 4407-4419 doi:10.1242/jcs.174359

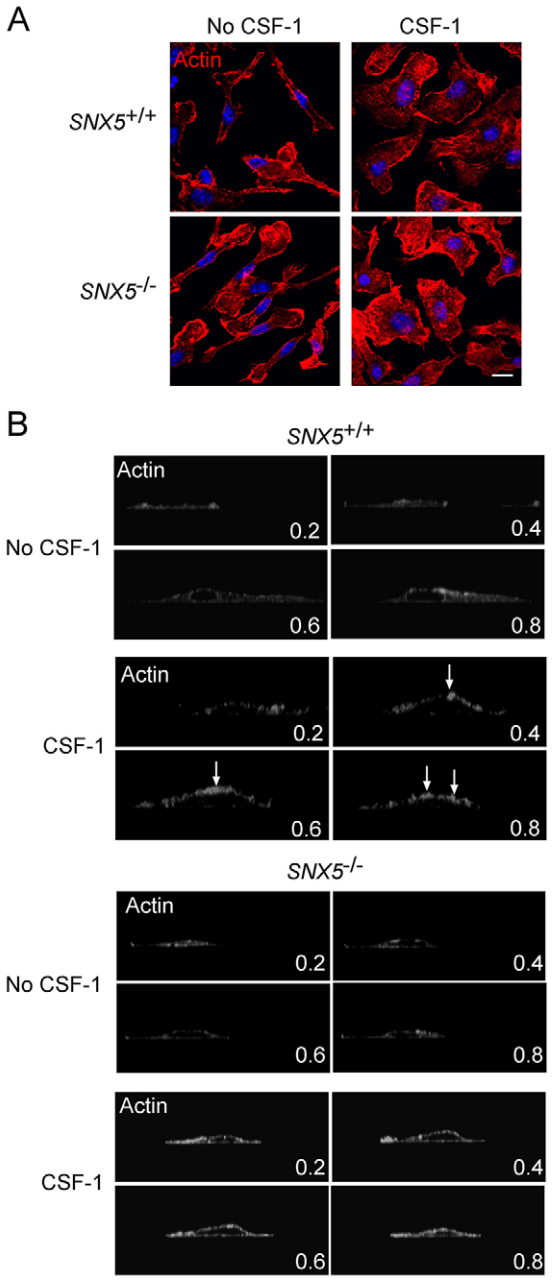

Fig. 6. Absence of SNX5 prevents the formation of actin-rich dorsal ruffles but not actin-rich peripheral ruffles in response to CSF-1 stimulation. (A) Peripheral ruffles. Quiescent BMMs from *SNX5*$^{+/+}$ (top panels) and *SNX5*$^{-/-}$ (bottom panels) mice were either stimulated with CSF-1 for 3 min at 37°C or left unstimulated, as indicated. Monolayers were then fixed, permeabilised and stained using TRITC–phalloidin (red) and DAPI (blue). Scale bar: 10 µm. (B) Dorsal ruffles. Quiescent BMMs from *SNX5*$^{+/+}$ (top panels) and *SNX5*$^{-/-}$ (bottom panels) mice were either stimulated with CSF-1 for 15 min at 37°C or left unstimulated, as indicated. Images are *x*-*z* cross-sections of fixed BMMs stained with TRITC–phalloidin. Images are a series of *x*-*z* cross-sections of fixed BMMs stained with TRITC–phalloidin across the width of the cell (number refers to the position of the cross section as a fraction of the total cell width). Arrows highlight the actin-stained dorsal ruffles on the *SNX5*$^{+/+}$ macrophage (top) compared to the lack of dorsal ruffles on *SNX5*$^{-/-}$ macrophage (bottom).

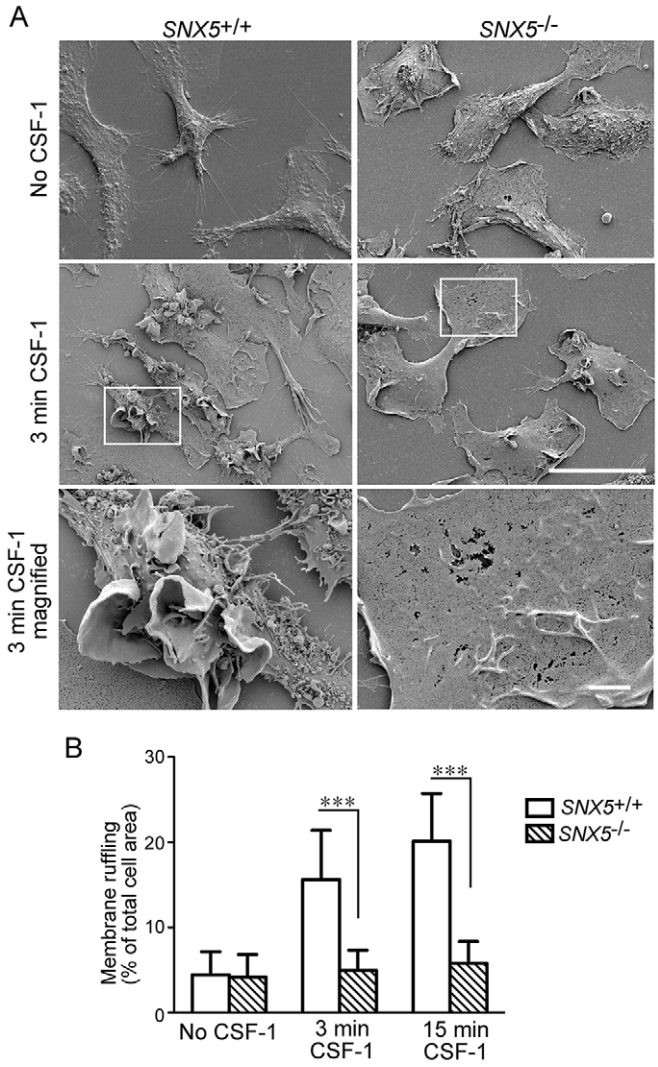

Fig. 7. Ultrastructural analysis of dorsal plasma membrane ruffles in the presence and absence of SNX5. BMMs from *SNX5*$^{+/+}$ and *SNX5*$^{-/-}$ mice were deprived of CSF-1 for 18 h and then either left unstimulated or stimulated with CSF-1 for 3 min (A,B) or 15 min (B). The cells were fixed with 0.4% glutaraldehyde and 4% paraformaldehyde in 0.1 M phosphate buffer for 16–18 h at 4°C, washed and dehydrated in graded ethanol solutions in water. The coverslips were dried and mounted on specimen stubs and coated with gold–palladium alloy. CSF-1-induced membrane ruffles were imaged using SEM (3500× magnification). Scale bar: 20 µm (top two rows), in magnified image, 2 µm. (B) Membrane ruffling was estimated by manually tracing the perimeter of the ruffles and measuring the area. The percentage ruffling for each cell was obtained by dividing the ruffling area by the sum of ruffling area and cell area (see Materials and Methods). The results shown are mean±s.d. of 30 cells from each population per time point over two independent experiments. ***P<0.001 (non-parametric Student's *t*-test).

macropinosomes than wild-type BMMs (data not shown). In addition, and more importantly, dorsal ruffles were detected by SEM in *SNX5*$^{-/-}$ BMMs transduced with adenovirus encoding GFP–SNX5 following CSF-1 activation (Fig. S2). Approximately 52% of transduced *SNX5*$^{-/-}$ BMMs cells were detected with dorsal ruffles, which is consistent with the transduction efficiency of ~65% as assessed by GFP fluorescence. In contrast, dorsal ruffles were not detected in CSF-1-stimulated BMMs from *SNX5*$^{-/-}$ mice transduced with adenovirus encoding GFP alone (Fig. S2). Given that dorsal ruffles are absent in *SNX5*$^{-/-}$ BMMs, these data show that the re-introduction of full-length SNX5 restores dorsal ruffles and macropinocytosis.

SNX5 and Arp3

Dorsal ruffles require actin branching, which is a coordinated response by a protein complex that includes Arp2/3. We initially

Journal of Cell Science (2015) 128, 4407-4419 doi:10.1242/jcs.174359

assessed the localisation of Arp3 to peripheral membrane ruffles in response to CSF-1 stimulation. After 3 min CSF-1 stimulation at 37°C, Arp3 was localised to actin-rich regions of the peripheral membrane ruffles of *SNX5*$^{+/+}$ BMMs as well as *SNX5*$^{-/-}$ BMMs (Fig. 8A), indicating that the localisation of Arp3 to the peripheral membrane ruffles is not dependent on SNX5. We then investigated the location of Arp3 on dorsal membrane ruffles in relation to SNX5. Here, we generated an orthogonal view of dorsal ruffles formed in *SNX5*$^{+/+}$ BMMs after 15 min CSF-1 stimulation (Fig. 8B). Endogenous SNX5 was localised to the base of actin-rich dorsal ruffles, juxtaposing closely with actin (Fig. 8B; actin+SNX5) and Arp3 on the same dorsal ruffles (Fig. 8B; SNX5+Arp3). SNX5 could also be observed in close proximity with Arp3 on actin-rich structures resembling macropinocytic cups 3 min after CSF-1 stimulation (Fig. S3).

In contrast, *SNX5*$^{-/-}$ BMMs lack dorsal ruffles and associated actin on the dorsal surface (Figs 6B and 7). One possibility is that the distribution of the CSF-1 receptors on the dorsal surface might differ between *SNX5*$^{+/+}$ and *SNX5*$^{-/-}$ BMMs, which could account for differences in spatial actin polymerisation. We assessed the distribution of CSF-1 receptors following activation. Upon 3 min stimulation with CSF-1, receptors on both *SNX5*$^{+/+}$ and *SNX5*$^{-/-}$ BMMs cluster into distinct microdomains on the dorsal surface of the macrophages (Fig. S4), suggesting that the localisation of CSF-1 receptor on the dorsal membrane is not influenced by SNX5 and that SNX5 functions downstream of CSF-1 receptor activation. Taken together, the data suggests that SNX5 can act in concert with the Arp2/3 complex to regulate the formation of CSF-1-stimulated dorsal ruffles on the plasma membrane from which macropinosomes can then be formed.

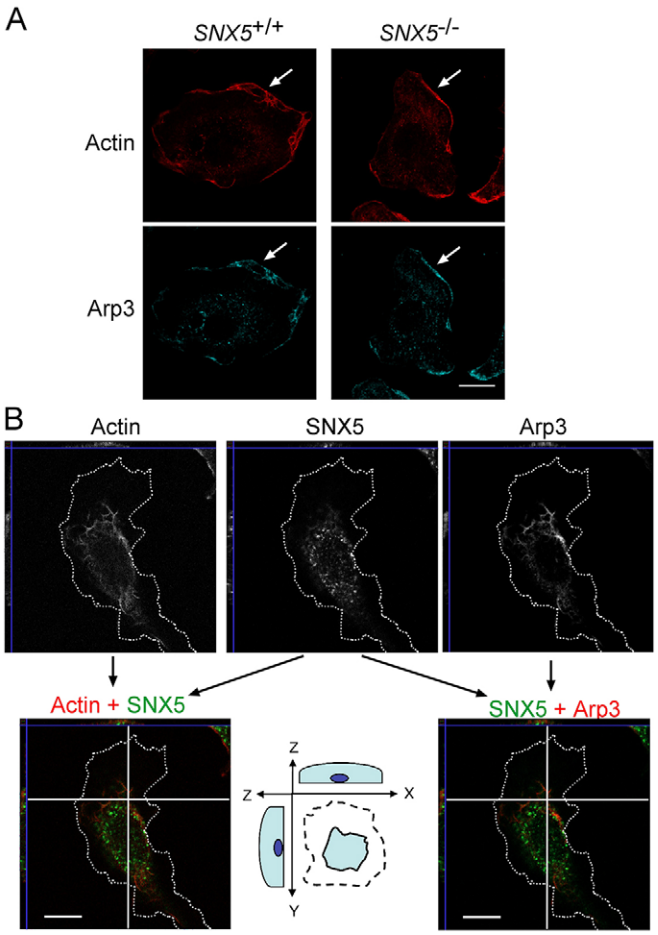

Fig. 8. Coordinated recruitment of SNX5 and Arp3 in actin cytoskeleton remodelling. (A,B) Quiescent *SNX5*$^{+/+}$ and *SNX5*$^{-/-}$ BMMs were either stimulated with CSF-1 for (A) 3 min at 37°C or (B) 15 min at 37°C. Monolayers were fixed and permeabilised, incubated with mouse BD Fc Block™ and then (A,B) stained with anti-Arp3 antibody followed by Alexa-Fluor-647-conjugated anti-mouse-IgG antibody and TRITC–phalloidin. In B, monolayers were also stained with anti-SNX5 antibody followed by Alexa-Fluor-488-conjugated anti-rabbit-IgG. *x-z* series of confocal images were scanned, pseudocoloured (as indicated) and orthogonal views generated using Volocity software. Scale bar, 10 µm.

DISCUSSION

Here, we have identified an essential role for SNX5 in the formation of macropinosomes derived from the dorsal ruffles of macrophages. Using mice deficient in SNX5 our findings show that: (1) macrophages lacking SNX5 have a dramatically reduced (60–70%) macropinocytic activity following CSF-1 activation compared with wild-type macrophages, (2) dendritic cells from SNX5-deficient mice have normal levels of macropinocytosis and antigen presentation, and (3) SNX5 is required for the formation of dorsal ruffles but not planar peripheral ruffles. Hence, our findings demonstrate that there are multiple pathways for macropinocytosis based on the type of membrane ruffling and, furthermore, that there are differences in the regulation of macropinocytosis between different immune cells. Moreover our study also clearly establishes the importance of dorsal ruffles in the generation of macropinosomes.

Mice deficient in SNX5 had normal life spans and were fertile. Other than a smaller size, there were no obvious developmental or physiological phenotype associated with the deletion of *SNX5*. Another report has described a SNX5-knockout mice which developed respiratory failure early in life (Im et al., 2013); however, these authors did not analyse macropinocytosis or dorsal ruffling in their mice. The phenotype observed by Im et al. (2013) was not observed in our SNX5-knockout mice. A major difference between the two studies is that the study by Im and colleagues (Im et al., 2013) targeted the *SNX5* gene in intron 7, which could result in the expression of a 26-kDa truncated protein that has the potential to act as a dominant negative mutant, whereas in our study *SNX5* was disrupted in intron 3. SNX5 has been reported to be involved in retromer-mediated endosomal sorting and endosome-to-Golgi retrograde trafficking (Wassmer et al., 2007, 2009). However, SNX5 is clearly not essential for these processes, at least in macrophages, as the retrograde trafficking of M6PR to the Golgi was unaffected by the absence of SNX5.

There are a number of common regulators of both macropinocytosis and phagocytosis, including dependence on PI3K and phosphatidylinositol-dependent recruitment of common effectors and adaptors (Swanson, 2008). However, phagocytosis was not affected by the lack of SNX5 in BMMs and moreover SNX5 was not detected on phagosomes in wild-type BMMs that had internalised insoluble zymogen particles. Hence, in macrophages at least, SNX5 is not recruited to the membranes of phagosomes and is a phosphatidylinositol-binding BAR domain protein that is selective for macropinosomes.

Previously, we noted that macropinocytosis was reduced but not completely blocked after silencing SNX5 in BMMs using microRNA (Lim et al., 2012). It was possible that the residual macropinocytic activity in this earlier study was due to incomplete silencing of SNX5. However, here we also observed a similar partial block in macropinocytosis in the complete absence of SNX5. The

Journal of Cell Science (2015) 128, 4407-4419 doi:10.1242/jcs.174359

block in fluid-phase endocytosis in SNX5-deficient macrophages was specific for the macropinocytosis pathway as phagocytosis and clathrin-mediated endocytosis were not affected by the absence of SNX5. The reduction in uptake of either 70 kDa dextran or ovalbumin by SNX5-deficient macrophages corresponded to the reduction in membrane ruffling of CSF-1-activated *SNX5*$^{-/-}$ macrophages compared with wild-type macrophages. Hence, the loss of membrane ruffling, and in particular dorsal ruffling, would appear to fully account for the reduced macropinocytic activity as measured by fluid-phase uptake assays.

The contribution of dorsal ruffling to macropinocytosis has been a subject of some debate (Buccione et al., 2004; Hoon et al., 2012; Suetsugu et al., 2003). Although SNX5 is found on macropinosomes derived from peripheral and dorsal ruffles, our findings indicate that SNX5 is essential only for dorsal-ruffle-derived macropinosomes. Only low levels of actin ruffling were detected on the dorsal membrane of SNX5-deficient macrophages as assessed by both light microscopy and SEM analysis. By contrast, microscopic analysis showed that peripheral ruffles were prominent in SNX5-deficient macrophages. Furthermore, the migration index of the *SNX5*$^{-/-}$ macrophages was similar to wild-type macrophages. As directed migration of cells is mediated from peripheral ruffles rather than dorsal ruffles (Suetsugu et al., 2003), these findings indicate that peripheral ruffling was not affected by the absence of SNX5. Therefore, our findings show that, following CSF-1 receptor activation in macrophages, the majority of macropinocytic activity is derived from dorsal ruffles. This conclusion is consistent with an emerging view that the dorsal surface and ruffles might function as a membrane domain specialised for signalling (Abella et al., 2010; Luo et al., 2014).

What is the role of SNX5 in promoting the generation of dorsal ruffles? Our previous work has shown that SNX5 binds both phosphatidylinositol 3-phosphate (PI3P) and PIP_2, the latter of which is derived from cell signalling events (Merino-Trigo et al., 2004) and that SNX5 is localised to newly emerging macropinosomes following receptor activation in HEK293 cells (Lim et al., 2008; Merino-Trigo et al., 2004). In this paper, we show that SNX5 is located at the plasma membrane following receptor activation of macrophages and that the plasma membrane localization of SNX5 is dependent on kinase activity of the CSF-1 receptor. Inhibition of tyrosine kinase activity has previously been shown to reduce macropinocytosis not only in macrophages but also in other cell types (Araki et al., 1996; Lim et al., 2008). Given that dorsal ruffles do not form in the absence of SNX5, our findings suggests that SNX5 is recruited to the plasma membrane, probably through an increase in PIP_2 production following receptor tyrosine kinase activation, to promote actin polymerisation and ruffle formation on the dorsal surface, which contributes to macropinocytosis. Our work shows that SNX5 is acting upstream of Arp2/3-mediated regulation of actin polymerisation and dorsal ruffling. Identification of the SNX5-binding partners in macrophages will be important to define the mechanism by which SNX5 co-ordinates dorsal ruffling. Using GFP–SNX5-expressing HeLa cells, SNX5 has previously been reported to interact with DOCK180 (also known as DOCK1), a GEF for the small GTPase Rac1, which is known to link extracellular signals to actin dynamics (Hara et al., 2008). However, we were unable to detect DOCK180 as a binding partner of endogenous SNX5 in activated macrophages from the analysis of pulldown experiments (J.P.L. and P.A.G., unpublished observations). Hence, it is likely that there are other, as yet undefined, binding partners involved in this process in macrophages. Finally, the BAR domain of SNX5 can regulate membrane curvature (Carlton et al., 2004; Peter et al., 2004), and this SNX5 domain might also be an important factor in regulating the membrane curvature required for macropinosome formation.

Immature dendritic cells are very active in macropinocytosis, which is a crucial pathway for their immune surveillance, and uptake and presentation of antigens (Lim and Gleeson, 2011; Mercer and Helenius, 2012; Norbury, 2006). Here, we found that, in contrast to macrophages, dendritic cells were unaffected by the lack of SNX5 and were able to present antigen as effectively to T cells as wild-type dendritic cells. Our study shows that there are differences in the regulation of the biogenesis of macropinocytosis between macrophages and dendritic cells. This difference might reflect the balance between constitutive and receptor-activated macropinocytosis because dendritic cells, and to a lesser extent macrophages, are able to macropinocytose constitutively. Recently constitutive ruffling and macropinocytosis has been shown to be a distinct pathway regulated by the elevated levels of phosphatidic acid in the plasma membrane of these cells (Bohdanowicz et al., 2013). These findings highlight the need to study and compare macropinocytosis in different primary cells.

Thus far, studies to identify the functional importance of macropinocytosis *in vivo* have used drugs such as amiloride, Sanglifehrin A or rapamycin (Hackstein et al., 2007, 2002; von Delwig et al., 2006). However, these drugs are not specific for macropinocytosis, which represents a major limitation in defining the role of macropinocytosis in a range of physiological processes *in vivo*. This study, which has identified SNX5 as a regulatory component of macropinocytosis derived from dorsal ruffles, will therefore provide a targeted approach to determine the effect of inhibiting one major pathway of macropinocytosis *in vivo*. In addition, and more broadly, the functions of dorsal ruffling, which have remained elusive (Hoon et al., 2012), will also be able to be directly investigated.

MATERIALS AND METHODS

Antibodies and reagents

CSF-1 was purchased from Life Technologies and Merck Millipore. Rabbit anti-mouse SNX5 antibody is as described previously (Lim et al., 2012). Rat anti-mouse CD16 and CD32 antibodies (Mouse BD Fc Block™), biotinylated hamster anti-mouse CD11c antibody and rat anti-mouse I-A/I-E MHCII antibody conjugated to PerCP-Cy5.5 were from BD Biosciences (USA). Mouse anti-human CD8a antibody, anti-mouse CD11c antibody conjugated to eFluor® 450 and anti-CD86 antibody conjugated to APC were obtained from eBioscience, USA. Rabbit anti-mouse GRASP65 antibody was from Abcam (UK), and Phalloidin–Tetramethylrhodamine B isothiocyanate (TRITC-Phalloidin) and mouse anti-Arp3 antibody were from Sigma-Aldrich (USA). Horseradish peroxidase (HRP)-conjugated swine anti-rabbit-IgG and rabbit anti-mouse-IgG antibodies were from DAKO Corporation (Denmark). Mouse monoclonal anti-bovine α-tubulin and goat anti-mouse-IgG antibody conjugated to Alexa Fluor 488, goat anti-mouse-IgG antibody conjugated to Alexa Fluor 647, goat anti-rabbit-IgG antibody conjugated to Alexa Fluor 488, goat anti-rabbit-IgG antibody conjugated to Alexa Fluor 568, goat anti-rabbit-IgG antibody conjugated to Alexa Fluor 647, Alexa-Fluor-488-labelled zymosan A bioparticles, lysine-fixable fluorescein isothiocynate (FITC)-conjugated 70 kDa dextran, DQ-ovalbumin and streptavidin conjugated with Alexa Fluor 647 were purchased from Life Technologies (USA). CSF-1 receptor tyrosine kinase inhibitor (GW2580) and rabbit anti-mouse CSF-1 receptor were purchased from Merck Millipore (USA).

Genotyping

The SNX5 'Knock-out First' mouse strain was created from an ESC clone (a2EPD0033_3_D07) and was obtained from the NCRR-NIH-supported KOMP repository and generated by the CSD consortium for the NIH-funded

Journal of Cell Science (2015) 128, 4407-4419 doi:10.1242/jcs.174359

KOMP project. Control ($SNX5^{+/+}$) mice used in all the experiments have the normal, unmodified SNX5 allele and are on the same C57BL/6 background as the $SNX5^{-/-}$ mice. Litters of weaned pups were genotyped using the following oligonucleotides: primer set 1, 5′-CTTTGCCTCTGATTTGGAT-CTCC-3′ and 5′-CTAAGACAATAAAACCCACCGGGCG-3′, to identify the SNX5 wild-type allele; and primer set 2, 5′-CCTCTTTAAAGGAAT-GAAGCCGTGGG-3′ and 5′-GAGATGGCGCAACGCAATTAAT-3′, to identify the SNX5 targeted allele. The annealing temperature for both PCR reactions was 53°C. All animal experiments were conducted according to government and institutional regulations and guidelines (University of Melbourne animal ethics approval 1212502.1).

Generation of BMMs

Eight- to 12-week-old mice were killed by CO_2 asphyxiation and BMMs were generated as previously described (Lim et al., 2012). Once generated, BMMs were cultured in RPMI supplemented with 10% (v/v) foetal calf serum, 100 units/ml penicillin, 100 g/ml streptomycin and 2 mM L-glutamine (complete RPMI medium).

Dendritic cell isolation

Dendritic cells were isolated from spleens as previously described (Moffat et al., 2013; Bourges et al., 2014). Dendritic cell isolation yielded preparations with ∼70–85% $CD11c^+$ purity. For antigen presentation assays, dendritic cells were activated by culture overnight in complete RPMI medium supplemented with 10 ng/ml granulocyte macrophage colony stimulating factor (GM-CSF, Peprotech).

Recombinant adenovirus constructs, production and transduction

Mouse SNX5 inserted at the C-terminus of GFP was as previously described (Lim et al., 2012). CD8–M6PR was amplified from pCMU-CD8/M6PR using primers which contain *EcoRI* and *XhoI* restrictions sites. The resulting PCR product was cloned into the *EcoRI*–*SalI* sites of pDC315 (Microbix Biosystems, Canada) for generating recombinant adenovirus (rADV). All constructs were verified by DNA sequencing. Production and transduction of recombinant adenovirus is as previously described (Lim et al., 2012).

Anti-CD8a internalisation

BMMs expressing CD8–M6PR constructs were chilled on ice for 5 min prior to incubation with pre-chilled Fc Block™ for 10 min. Fc Block™ was then removed and replaced with anti-CD8a antibodies (eBioscience, USA), diluted 1:100 in serum-free RPMI, on ice for 30 min. Unbound antibodies were removed using cold PBS washes and the internalisation of antibody-bound CD8–M6PR was performed in serum-free RPMI for the indicated duration at 37°C. Cells were fixed with 4% (w/v) paraformaldehyde and processed for immunofluorescence.

Phagocytosis

BMMs at density of 2×10^5 cells/ml were cultured overnight in complete RPMI medium in the absence of CSF-1, washed in serum-free medium, and incubated with 7×10^5 particles/ml and 1.6×10^5 particles/ml of Alexa-Fluor-488-labelled zymosan A bioparticles at 37°C for 60 min. Non-phagocytosed zymosan particles were removed with ice-cold PBS washes, cell monolayers fixed and processed for immunofluorescence. Monolayers were counterstained with TRITC–phalloidin and the number of fluorescent particles per cell was then scored for triplicate experiments of 50 cells each.

Fluid-phase uptake assays

BMMs

BMMs at a density of 2×10^5 cells/ml were cultured overnight in complete RPMI medium in the absence of CSF-1 to render macrophages quiescent. Then, macrophages were incubated with 500 µg/ml fluorescently conjugated 70 kDa dextran in the presence of 50 ng/ml of CSF-1 in serum-free RPMI at 37°C for various times as indicated. Following the incubation, cells were placed on ice for 5 min to inhibit uptake of dextran and cells were then washed with cold complete RPMI and PBS. Control incubations were also performed on ice. Cells were either processed for immunofluorescence or analysed live by flow cytometry. Pulse-chase with DQ-ovalbumin was performed as described (Lim et al., 2012).

For flow cytometry after dextran uptake, BMMs were incubated with 10 mM EDTA on ice for 10–15 min and then gently scraped off Petri dishes. Cells were washed twice in cold PBS containing 0.1% BSA (w/v) and 2 mM EDTA. Cells were then subjected to an acid-salt wash (0.5 M NaCl, 0.2 M acetic acid, pH 3), to remove dextran non-specifically bound to the cell surface, and washed again prior to flow cytometry using a FACSort (Becton-Dickinson, California, USA).

Splenic dendritic cells

1.8×10^6 Nycodenz-enriched dendritic cells were incubated with 1 mg/ml fluorescently conjugated 70 kDa dextran in 200 µl of serum-free RPMI. Cells were then washed four times in PBS containing 0.1% (w/v) BSA and 2 mM EDTA. For immunofluorescence microscopy, cells were stained with biotinylated hamster anti-mouse CD11c antibody followed by streptavidin-conjugated Alexa Fluor 647, and cell suspensions were pelleted onto microscope slides using a CytoSpin and stained with DAPI. For flow cytometry, live cells were stained with anti-CD11c antibody conjugated to eFluor® 450, anti-CD86 antibody conjugated to APC and anti-MHCII antibody conjugated to PerCP-Cy5.5 prior to flow cytometry analysis on a LSR Fortessa (BD Biosciences).

Antigen presentation assay

Antigen presentation assays with mouse spleen dendritic cells involved dendritic cell isolation and incubation with antigen. Dendritic cells were pulsed with OVA protein (Worthington Biochemicals) in the presence of fully phosphorothioated 0.5 mM CpG 1668, type B (custom made, Geneworks) for 45 min at 37°C. Antigen-pulsed dendritic cells were incubated with Cell Trace Violet (Invitrogen) labelled OT-II transgenic T cells for 64 h in complete RPMI medium supplemented with 10 ng/ml GM-CSF (Peprotech). T cell division was assessed by flow cytometry. Cell number was determined by inclusion of calibration particles (BD Biosciences).

Immunofluorescence and microscopy

Cells were fixed in 4% (w/v) paraformaldehyde, permeabilised and processed for immunofluorescence as previously described (Chia et al., 2011). Unless otherwise indicated, cells were examined using a Leica TCS SP2 system and Leica Confocal Software version 2.61. For multi-colour labelling, images were collected independently. Images were analysed using Metamorph Version 7.5.6.0 software or Volocity 6.3 software (Perkin Elmer).

Surface CSF-1 receptor level

BMMs cultured overnight in complete RPMI medium in the absence of CSF-1 were lifted from Petri dishes by incubating in 10 mM EDTA on ice for 15 min. Cells were then washed in cold PBS containing 0.1% (w/v) BSA and 2 mM EDTA. BMMs was stained with rabbit anti-mouse CSF-1R antibody for 30 min on ice followed by Alexa-Fluor-488-conjugated anti-rabbit-IgG antibody and analysed by flow cytometry.

Inhibition of CSF-1 receptor tyrosine kinase

BMMs that had been cultured overnight in in complete RMPI medium in the absence of CSF-1 to render macrophages quiescent were pre-treated with 5 µM of 5-{3-Methoxy-4-[(4-methoxybenzyl)oxy]benzyl}-pyrimidine-2,4-diamine (GW2580) or DMSO (carrier control) for 1 h at 37°C prior to dextran uptake assays or stimulation with CSF-1.

Transwell migration assay

BMMs were cultured overnight in the absence of CSF-1 to render macrophages quiescent. Cells were then harvested by gentle scraping and resuspended in complete RPMI at 2×10^6 cells/ml. Cell suspensions (150 µl) in complete RPMI were seeded onto the upper chamber of a transwell insert containing an 8-µm pore size Polyethylene Terephthalate membrane (24-well Millicell Hanging Cell Culture inserts, Millipore, Switzerland). The lower chamber contained either complete RPMI or supplemented with 50 ng/ml CSF-1. After 4 h incubation at 37°C, cells that had not migrated were removed with a cotton swab and the transwell inserts washed four times

with PBS. Cells that had migrated to the lower surface of the membrane were fixed in 4% paraformaldehyde and stained with DAPI. The experiments were performed in triplicate and the number of migrating cells in five fields per membrane was counted microscopically at 100× magnification. Data were expressed as the migration index (number of cells migrated to the underside of the membrane in the presence of CSF-1/number of cells migrated in the absence of CSF-1).

Scanning electron microscopy

BMMs grown on 22-mm square glass coverslips were fixed with 0.4% gluteraldehyde and 4% paraformaldehyde in 0.1 M phosphate buffer, pH 7.4, for 16–18 h at 4°C. The coverslips were then rinsed in 0.1 M phosphate buffer followed by three PBS washes. The coverslips were then dehydrated in graded ethanol solutions in water (10%, 30%, 50%, 70%, 90%, 100% for 10 min each); 2×100% ethanol (10 min each). The coverslips were dried using a critical point dryer (Balzers CPD 030). The samples were then mounted on specimen stubs and coated with a gold–palladium alloy using a Dynavac Xenospot gold coater. The presence of membrane ruffling was examined using a Philips XL 30 FEG, field emission SEM with an accelerating voltage of 2 kV. All measurements necessary to quantify the CSF-1-induced responses were performed using ImageJ software. The percentage ruffling for each cell was obtained by dividing the ruffling area by the sum of ruffling area (R) and cell area (C) as (R×100)/(R+C) (Chitu et al., 2005).

Immunoblotting

Immunoblotting performed as previously described (Lim et al., 2012).

Statistical analysis

The unpaired two-tailed Student *t*-test was used to determine statistical significance. A *P*-value of 0.05 (*) was considered as significant, a *P*-value of <0.01(**) was highly significant and a *P*-value of <0.001 (***) was very highly significant. The absence of a *P*-value indicates the differences were not significant.

Acknowledgements

We thank Fiona Houghton for expert technical advice and Dr Simon Crawford, School of Botany, University of Melbourne for assistance with SEM sample preparation. The authors acknowledge the assistance of The Biological Optical Microscopy at the University of Melbourne.

Competing interests

The authors declare no competing or financial interests.

Author contributions

Experiments were designed by J.P.L. and P.A.G. BMM experiments were performed by J.P.L., dendritic cell experiments by J.D.M., E.M.R. and J.P.L., SEM by P.G. The paper was written by J.P.L. and P.A.G.

Funding

This work was supported by funding from the National Health and Medical Research Council of Australia [grant number ID566727].

Supplementary information

Supplementary information available online at
http://jcs.biologists.org/lookup/suppl/doi:10.1242/jcs.174359/-/DC1

References

Abella, J. V., Parachoniak, C. A., Sangwan, V. and Park, M. (2010). Dorsal ruffle microdomains potentiate Met receptor tyrosine kinase signaling and down-regulation. *J. Biol. Chem.* **285**, 24956-24967.

Amyere, M., Payrastre, B., Krause, U., Van Der Smissen, P., Veithen, A. and Courtoy, P. J. (2000). Constitutive macropinocytosis in oncogene-transformed fibroblasts depends on sequential permanent activation of phosphoinositide 3-kinase and phospholipase C. *Mol. Biol. Cell* **11**, 3453-3467.

Anzinger, J. J., Chang, J., Xu, Q., Barthwal, M. K., Bohnacker, T., Wymann, M. P. and Kruth, H. S. (2012). Murine bone marrow-derived macrophages differentiated with GM-CSF become foam cells by PI3Kgamma-dependent fluid-phase pinocytosis of native LDL. *J. Lipid Res.* **53**, 34-42.

Araki, N., Johnson, M. T. and Swanson, J. A. (1996). A role for phosphoinositide 3-kinase in the completion of macropinocytosis and phagocytosis by macrophages. *J. Cell Biol.* **135**, 1249-1260.

Bohdanowicz, M., Schlam, D., Hermansson, M., Rizzuti, D., Fairn, G. D., Ueyama, T., Somerharju, P., Du, G. and Grinstein, S. (2013). Phosphatidic acid is required for the constitutive ruffling and macropinocytosis of phagocytes. *Mol. Biol. Cell* **24**, 1700-1712, S1-7.

Bourges, D., Ross, E. M., Allen, S., Read, S., Houghton, F. J., Bedoui, S., Boon, L., Gleeson, P. A. and van Driel, I. R. (2014). Transient systemic inflammation does not alter the induction of tolerance to gastric autoantigens by migratory dendritic cells. *J. Immunol.* **192**, 5023-5030.

Buccione, R., Orth, J. D. and McNiven, M. A. (2004). Foot and mouth: podosomes, invadopodia and circular dorsal ruffles. *Nat. Rev. Mol. Cell Biol.* **5**, 647-657.

Carlton, J., Bujny, M., Peter, B. J., Oorschot, V. M. J., Rutherford, A., Mellor, H., Klumperman, J., McMahon, H. T. and Cullen, P. J. (2004). Sorting nexin-1 mediates tubular endosome-to-TGN transport through coincidence sensing of high- curvature membranes and 3-phosphoinositides. *Curr. Biol.* **14**, 1791-1800.

Chia, P. Z. C., Gasnereau, I., Lieu, Z. Z. and Gleeson, P. A. (2011). Rab9-dependent retrograde transport and endosomal sorting of the endopeptidase furin. *J. Cell Sci.* **124**, 2401-2413.

Chitu, V., Pixley, F. J., Macaluso, F., Larson, D. R., Condeelis, J., Yeung, Y.-G. and Stanley, E. R. (2005). The PCH family member MAYP/PSTPIP2 directly regulates F-actin bundling and enhances filopodia formation and motility in macrophages. *Mol. Biol. Cell* **16**, 2947-2959.

Clague, M. J., Thorpe, C. and Jones, A. T. (1995). Phosphatidylinositol 3-kinase regulation of fluid phase endocytosis. *FEBS Lett.* **367**, 272-274.

Cullen, P. J. (2008). Endosomal sorting and signalling: an emerging role for sorting nexins. *Nat. Rev. Mol. Cell Biol.* **9**, 574-582.

Daro, E., Pulendran, B., Brasel, K., Teepe, M., Pettit, D., Lynch, D. H., Vremec, D., Robb, L., Shortman, K., McKenna, H. J. et al. (2000). Polyethylene glycol-modified GM-CSF expands CD11b(high)CD11c(high) but notCD11b(low)CD11c (high) murine dendritic cells in vivo: a comparative analysis with Flt3 ligand. *J. Immunol.* **165**, 49-58.

Dharmawardhane, S., Schurmann, A., Sells, M. A., Chernoff, J., Schmid, S. L. and Bokoch, G. M. (2000). Regulation of macropinocytosis by p21-activated kinase-1. *Mol. Biol. Cell* **11**, 3341-3352.

Feliciano, W. D., Yoshida, S., Straight, S. W. and Swanson, J. A. (2011). Coordination of the Rab5 cycle on macropinosomes. *Traffic* **12**, 1911-1922.

Hackstein, H., Taner, T., Logar, A. J. and Thomson, A. W. (2002). Rapamycin inhibits macropinocytosis and mannose receptor-mediated endocytosis by bone marrow-derived dendritic cells. *Blood* **100**, 1084-1087.

Hackstein, H., Steinschulte, C., Fiedel, S., Eisele, A., Rathke, V., Stadlbauer, T., Taner, T., Thomson, A. W., Tillmanns, H., Bein, G. et al. (2007). Sanglifehrin a blocks key dendritic cell functions in vivo and promotes long-term allograft survival together with low-dose CsA. *Am. J. Transplant.* **7**, 789-798.

Haigler, H. T., McKanna, J. A. and Cohen, S. (1979). Rapid stimulation of pinocytosis in human carcinoma cells A-431 by epidermal growth factor. *J. Cell Biol.* **83**, 82-90.

Hara, S., Kiyokawa, E., Iemura, S.-i., Natsume, T., Wassmer, T., Cullen, P. J., Hiai, H. and Matsuda, M. (2008). The DHR1 domain of DOCK180 binds to SNX5 and regulates cation-independent mannose 6-phosphate receptor transport. *Mol. Biol. Cell* **19**, 3823-3835.

Hewlett, L. J., Prescott, A. R. and Watts, C. (1994). The coated pit and macropinocytic pathways serve distinct endosome populations. *J. Cell Biol.* **124**, 689-703.

Hoon, J.-L., Wong, W.-K. and Koh, C.-G. (2012). Functions and regulation of circular dorsal ruffles. *Mol. Cell. Biol.* **32**, 4246-4257.

Im, S.-K., Jeong, H., Jeong, H.-W., Kim, K.-T., Hwang, D., Ikegami, M. and Kong, Y.-Y. (2013). Disruption of sorting nexin 5 causes respiratory failure associated with undifferentiated alveolar epithelial type I cells in mice. *PLoS ONE* **8**, e58511.

Jones, G. E. (2000). Cellular signaling in macrophage migration and chemotaxis. *J. Leukoc. Biol.* **68**, 593-602.

Kerr, M. C., Lindsay, M. R., Luetterforst, R., Hamilton, N., Simpson, F., Parton, R. G., Gleeson, P. A. and Teasdale, R. D. (2006). Visualisation of macropinosome maturation by the recruitment of sorting nexins. *J. Cell Sci.* **119**, 3967-3980.

Kerr, M. C., Wang, J. T. H., Castro, N. A., Hamilton, N. A., Town, L., Brown, D. L., Meunier, F. A., Brown, N. F., Stow, J. L. and Teasdale, R. D. (2010). Inhibition of the PtdIns(5) kinase PIKfyve disrupts intracellular replication of Salmonella. *EMBO J.* **29**, 1331-1347.

Lee, E. and Knecht, D. A. (2002). Visualization of actin dynamics during macropinocytosis and exocytosis. *Traffic* **3**, 186-192.

Lieu, Z. Z., Derby, M. C., Teasdale, R. D., Hart, C., Gunn, P. and Gleeson, P. A. (2007). The golgin GCC88 is required for efficient retrograde transport of cargo from the early endosomes to the trans-golgi network. *Mol. Biol. Cell* **18**, 4979-4991.

Lim, J. P. and Gleeson, P. A. (2011). Macropinocytosis: an endocytic pathway for internalising large gulps. *Immunol. Cell Biol.* **89**, 836-843.

Lim, J. P., Wang, J. T. H., Kerr, M. C., Teasdale, R. D. and Gleeson, P. A. (2008). A role for SNX5 in the regulation of macropinocytosis. *BMC Cell Biol.* **9**, 58.

Lim, J. P., Teasdale, R. D. and Gleeson, P. A. (2012). SNX5 is essential for efficient macropinocytosis and antigen processing in primary macrophages. *Biol. Open* **1**, 904-914.

Luo, L., Wall, A. A., Yeo, J. C., Condon, N. D., Norwood, S. J., Schoenwaelder, S., Chen, K. W., Jackson, S., Jenkins, B. J., Hartland, E. L. et al. (2014). Rab8a interacts directly with PI3Kgamma to modulate TLR4-driven PI3K and mTOR signalling. *Nat. Commun.* **5**, 4407.

May, R. C. and Machesky, L. M. (2001). Phagocytosis and the actin cytoskeleton. *J. Cell Sci.* **114**, 1061-1077.

Mercer, J. and Helenius, A. (2012). Gulping rather than sipping: macropinocytosis as a way of virus entry. *Curr. Opin. Microbiol.* **15**, 490-499.

Merino-Trigo, A., Kerr, M. C., Houghton, F., Lindberg, A., Mitchell, C., Teasdale, R. D. and Gleeson, P. A. (2004). Sorting nexin 5 is localized to a subdomain of the early endosomes and is recruited to the plasma membrane following EGF stimulation. *J. Cell Sci.* **117**, 6413-6424.

Moffat, J. M., Cheong, W.-S., Villadangos, J. A., Mintern, J. D. and Netter, H. J. (2013). Hepatitis B virus-like particles access major histocompatibility class I and II antigen presentation pathways in primary dendritic cells. *Vaccine* **31**, 2310-2316.

Norbury, C. C. (2006). Drinking a lot is good for dendritic cells. *Immunology* **117**, 443-451.

Norbury, C. C., Hewlett, L. J., Prescott, A. R., Shastri, N. and Watts, C. (1995). Class I MHC presentation of exogenous soluble antigen via macropinocytosis in bone marrow macrophages. *Immunity* **3**, 783-791.

Norbury, C. C., Chambers, B. J., Prescott, A. R., Ljunggren, H.-G. and Watts, C. (1997). Constitutive macropinocytosis allows TAP-dependent major histocompatibility complex class I presentation of exogenous soluble antigen by bone marrow-derived dendritic cells. *Eur. J. Immunol.* **27**, 280-288.

Patel, P. C. and Harrison, R. E. (2008). Membrane ruffles capture C3bi-opsonized particles in activated macrophages. *Mol. Biol. Cell* **19**, 4628-4639.

Peter, B. J., Kent, H. M., Mills, I. G., Vallis, Y., Butler, P. J., Evans, P. R. and McMahon, H. T. (2004). BAR domains as sensors of membrane curvature: the amphiphysin BAR structure. *Science* **303**, 495-499.

Racoosin, E. L. and Swanson, J. A. (1989). Macrophage colony-stimulating factor (rM-CSF) stimulates pinocytosis in bone marrow-derived macrophages. *J. Exp. Med.* **170**, 1635-1648.

Roberts, R. L., Barbieri, M. A., Ullrich, J. and Stahl, P. D. (2000). Dynamics of rab5 activation in endocytosis and phagocytosis. *J. Leukoc. Biol.* **68**, 627-632.

Sallusto, F., Cella, M., Danieli, C. and Lanzavecchia, A. (1995). Dendritic cells use macropinocytosis and the mannose receptor to concentrate macromolecules in the major histocompatibility complex class II compartment: downregulation by cytokines and bacterial products. *J. Exp. Med.* **182**, 389-400.

Sampaio, N. G., Yu, W., Cox, D., Wyckoff, J., Condeelis, J., Stanley, E. R. and Pixley, F. J. (2011). Phosphorylation of CSF-1R Y721 mediates its association with PI3K to regulate macrophage motility and enhancement of tumor cell invasion. *J. Cell Sci.* **124**, 2021-2031.

Santambrogio, L., Sato, A. K., Carven, G. J., Belyanskaya, S. L., Strominger, J. L. and Stern, L. J. (1999). Extracellular antigen processing and presentation by immature dendritic cells. *Proc. Natl. Acad. Sci. USA* **96**, 15056-15061.

Seaman, M. N. J. (2004). Cargo-selective endosomal sorting for retrieval to the Golgi requires retromer. *J. Cell Biol.* **165**, 111-122.

Skarnes, W. C., Rosen, B., West, A. P., Koutsourakis, M., Bushell, W., Iyer, V., Mujica, A. O., Thomas, M., Harrow, J., Cox, T. et al. (2011). A conditional knockout resource for the genome-wide study of mouse gene function. *Nature* **474**, 337-342.

Suetsugu, S., Yamazaki, D., Kurisu, S. and Takenawa, T. (2003). Differential roles of WAVE1 and WAVE2 in dorsal and peripheral ruffle formation for fibroblast cell migration. *Dev. Cell* **5**, 595-609.

Swanson, J. A. (1989). Phorbol esters stimulate macropinocytosis and solute flow through macrophages. *J. Cell Sci.* **94**, 135-142.

Swanson, J. A. (2008). Shaping cups into phagosomes and macropinosomes. *Nat. Rev. Mol. Cell Biol.* **9**, 639-649.

Swanson, J. A. and Watts, C. (1995). Macropinocytosis. *Trends Cell Biol.* **5**, 424-428.

Villadangos, J. A. and Schnorrer, P. (2007). Intrinsic and cooperative antigen-presenting functions of dendritic-cell subsets in vivo. *Nat. Rev. Immunol.* **7**, 543-555.

von Delwig, A., Hilkens, C. M. U., Altmann, D. M., Holmdahl, R., Isaacs, J. D., Harding, C. V., Robertson, H., McKie, N. and Robinson, J. H. (2006). Inhibition of macropinocytosis blocks antigen presentation of type II collagen in vitro and in vivo in HLA-DR1 transgenic mice. *Arthritis Res. Ther.* **8**, R93.

Wang, J. T. H., Kerr, M. C., Karunaratne, S., Jeanes, A., Yap, A. S. and Teasdale, R. D. (2010). The SNX-PX-BAR family in macropinocytosis: the regulation of macropinosome formation by SNX-PX-BAR proteins. *PLoS ONE* **5**, e13763.

Wassmer, T., Attar, N., Bujny, M. V., Oakley, J., Traer, C. J. and Cullen, P. J. (2007). A loss-of-function screen reveals SNX5 and SNX6 as potential components of the mammalian retromer. *J. Cell Sci.* **120**, 45-54.

Wassmer, T., Attar, N., Harterink, M., van Weering, J. R., Traer, C. J., Oakley, J., Goud, B., Stephens, D. J., Verkade, P., Korswagen, H. C. et al. (2009). The retromer coat complex coordinates endosomal sorting and dynein-mediated transport, with carrier recognition by the trans-Golgi network. *Dev. Cell* **17**, 110-122.

Yoshida, S., Hoppe, A. D., Araki, N. and Swanson, J. A. (2009). Sequential signaling in plasma-membrane domains during macropinosome formation in macrophages. *J. Cell Sci.* **122**, 3250-3261.